Research Square

Preprints are preliminary reports that have not undergone peer review.
They should not be considered conclusive, used to inform clinical practice,
or referenced by the media as validated information.

Classification of brain tumors using pseudobulk spatial transcriptomics

Sze Jet Aw

aw.sze.jet@singhealth.com.sg

KK Women's and Children's Hospital

Chuan Keng Goh

KK Women's and Children's Hospital

Jian Yuan Goh

KK Women's and Children's Hospital

Debbra Yi Xin Chong

KK Women's and Children's Hospital

Enrica Ee Kar Tan

KK Women's and Children's Hospital

Sharon Yin Yee Low

KK Women's and Children's Hospital

Research Article

Keywords: spatial transcriptomics, pseudobulk, brain tumor classification, tissue conservation, tumor-cluster enrichment

Posted Date: November 12th, 2026

DOI: https://doi.org/10.21203/rs.3.rs-11458349/v1

License: This work is licensed under a Creative Commons Attribution 4.0 International License.
Read Full License

Additional Declarations: No competing interests reported.

Classification of brain tumors using pseudobulk spatial transcriptomics

Authors

Sze Jet Aw[1*]

Chuan Keng Goh[1]

Jian Yuan Goh[1]

Debbra Yi Xin Chong[2]

Enrica Ee Kar Tan[2]

Sharon Yin Yee Low[3]

Affiliations

[1] Department of Pathology and Laboratory Medicine, KK Women's and Children's Hospital,100 Bukit Timah Road, Singapore 229899, Singapore

[2] Paediatric Haematology/Oncology Service, KK Women's and Children's Hospital, 100 Bukit Timah Road, Singapore 229899, Singapore

[3] Neurosurgical Service, KK Women's and Children's Hospital, 100 Bukit Timah Road, Singapore 229899, Singapore

Corresponding author:

Sze Jet Aw

Email: aw.sze.jet@singhealth.com.sg

Telephone: +65 394 8748

Street Address: Department of Pathology and Laboratory Medicine, Children's Tower, Basement 1, 100 Bukit Timah Road, Singapore 229899

Word count: 4,512 (title page, abstract, text and references) 6,112 including four figures at 400 words each

Author contributions

S.J.A. designed the study, developed the analysis pipeline, and performed the classification analyses; D.Y.X.C., E.E.K.T., and S.Y.Y.L. contributed the institutional cases, clinical data and reference diagnoses; C.K.G. provided technical support for preparation of institutional cases for Visium HD analysis; J.Y.G. provided data curation and interpretation. All authors reviewed and approved the final manuscript.

Abstract

Transcriptomic classification of central nervous system (CNS) tumors is emerging as a diagnostic adjunct. However, conventional bulk sequencing requires multiple tissue sections, which is challenging when biopsy material is limited or diffuse infiltration dilutes the neoplastic signal. Spatial transcriptomics can interrogate gene expression from a single tissue section and computationally isolate tumor-enriched regions, but its compatibility with existing bulk-trained

transcriptomic classifiers has not been systematically evaluated. We developed a standardized pipeline to generate pseudobulk expression profiles from Visium spatial transcriptomics data and applied three classifiers (a correlation-based k-nearest neighbor [kNN], M&M, and OTTER) to 79 publicly available CNS tumor datasets and 5 institutional Visium HD cases multiplexed onto a single slide. The kNN classifier achieved the highest concordance with reference diagnoses (82.3%), followed by M&M (60.3%) and OTTER (46.5%). Medulloblastoma and ependymoma achieved near-perfect concordance, while high-grade gliomas were the most challenging. Formalin fixation reduced performance, most markedly for OTTER. In cases with low kNN confidence, tumor-cluster enrichment improved concordance from 60% to 76%. Pseudobulk aggregation of spatial transcriptomics data from a single tissue section can therefore yield diagnostically informative classifications using existing classifiers, with potential for tissue-limited specimens and infiltrative tumors.

Keywords: spatial transcriptomics; pseudobulk; brain tumor classification; tissue conservation; tumor-cluster enrichment

Introduction

Increasing access to molecular techniques has augmented brain tumor classification beyond histomorphology alone. DNA methylation profiling is considered routine in resource-enabled laboratories and is necessary for the classification of certain tumor types.[15] Another emerging approach is transcriptomic classification where several models published in recent years report equivalent capabilities compared with methylation-based methods.[5,14,7] However, molecular testing faces tissue volume constraints and issues of tumor purity. This is particularly acute in neuropathology, where several diagnostic settings routinely yield minimal material such as

stereotactic biopsy of brainstem lesions, endoscopic biopsy of pineal region tumors, and sampling of intramedullary spinal cord. The problem is further compounded by diffuse growth patterns that hinder isolation of a pure neoplastic population for molecular analysis.

Spatial transcriptomic sequencing has emerged as a modality capable of interrogating a tissue's transcriptome at a spatially resolved, near-single-cell level from a single tissue section.[11,12] Critically, these platforms allow computational isolation of tumor-enriched regions in silico, minimizing dilution by admixed non-neoplastic tissue. However, it remains uncertain whether the expression profiles generated by spatial transcriptomics are sufficiently compatible with existing bulk-trained classifiers to yield diagnostically useful results.

We therefore asked whether spatial transcriptomics aggregated into a pseudobulk format can drive existing transcriptomic classifiers from a single tissue section. A standardized pipeline was designed to generate pseudobulk profiles from publicly available Visium brain tumor datasets, and thereafter applied to three classifiers of distinct architecture: a correlation-based k-nearest neighbor (kNN) classifier built on a recently published transcriptomic atlas of nervous system tumors,[7] the M&M ensemble classifier,[14] and OTTER.[5] We assessed concordance with reference diagnoses across diagnostic categories and tissue preservation types, tested whether spatial isolation of tumor-enriched clusters could improve classification in sub-threshold cases, and applied the pipeline to multiplexed institutional Visium HD cases as an illustrative case series.

Materials and methods

Ethics approval and consent to participate

This study was approved by the SingHealth Institutional Review Board (CIRB Ref: 2014-2079). Written informed consent for research use of tissue was obtained from the parents or legal

guardians of the patients whose institutional cases were included. The publicly available datasets used in this study were obtained from published sources and did not require additional ethics approval. Consent for publication was obtained from the parents or legal guardians of the patients whose institutional cases were included.

Study Cohort

A total of 101 publicly available Visium spatial transcriptomics datasets were assembled from Zenodo (DOI: 10.5281/zenodo.10863259 and 10.5281/zenodo.14064047), Dryad (DOI: 10.5061/dryad.h70rxwdmj) and GEO (GSE195661). Twenty-two cases were excluded because of incomplete diagnostic annotation, leaving 79 cases for analysis. These comprised 47 high-grade gliomas, 14 ependymomas, 8 low-grade gliomas/glioneuronal tumors, 4 medulloblastomas, and 6 non-neoplastic control tissue samples (Online Resource 4).

Of the 79 cases, 48 were derived from fresh-frozen (FF) tissue and 30 from formalin-fixed paraffin-embedded (FFPE) tissue. One case (UKF269_T_ST) carried an ambiguous FF/FFPE annotation and was excluded from preservation-type analyses.

An additional five fresh-frozen institutional cases were multiplexed onto a single 10x Genomics (Pleasanton, CA, USA) Visium HD 6.5 mm slide and profiled using the Visium HD 3' Spatial Gene Expression platform. These comprised two medulloblastomas (group 3 and group 4), a diffuse pediatric-type high-grade glioma (H3-wildtype, IDH-wildtype), an astroblastoma with *MN1::BEND2* fusion, and a previously reported embryonal tumor with *BRD4::CTRC1* fusion and *BCOR* internal tandem duplication.[2] Library preparation details, tumor region isolation and pseudobulk generation for these cases are provided in Online Resource 1.

Whole-Slide Pseudobulk Generation and Quality Control

A standardized computational pipeline was developed in Python (v3.11) using Scanpy (v1.11.5) to generate pseudobulk expression profiles from all spatial transcriptomic datasets.[17] In the primary analysis, all spots within each dataset were aggregated into a single whole-slide pseudobulk profile without prior cluster selection or spatial subsetting.

Feature–barcode matrices were loaded and gene names deduplicated. Spots were retained if they expressed ≥200 genes, contained ≥500 total UMI counts, and had ≤20% mitochondrial transcripts. Genes detected in fewer than 3 spots were removed, and spots not overlying tissue were excluded where spatial position annotations were available. Thresholds were held constant across the 79 public datasets; adjusted values for the institutional cases are given in Online Resource 1. After filtering, a whole-slide pseudobulk profile was generated for each sample by summing raw (unnormalized) counts across all retained spots.

Classifier Input Preparation

Three classifier-specific adapter modules converted the standardized raw count vector into the format required by each tool; preprocessing was therefore identical across the three classifiers. The pseudobulk counts were then processed by the three different classifiers (see Online Resource 1 for details).

Concordance Assessment

Reference diagnostic labels were derived from the histopathological and molecular annotations provided by the original source publications for each dataset. These were mapped to five harmonized diagnostic categories with reference to the 2021 WHO Classification of Tumors of the

Central Nervous System: high-grade glioma, low-grade glioma/glioneuronal tumor, ependymoma, medulloblastoma and control tissue.[15] The constituent entities of each category, and the mapping of finer classifier subtype labels, are listed in Online Resource 2. Subgroup-level predictions were assessed where reference annotation permitted.

Tumor-Cluster Enrichment Strategy

To assess whether spatial isolation of tumor-predominant regions could rescue sub-optimal classifications, a second-pass tumor-cluster enrichment strategy was applied to a targeted subset of cases. Enrichment was evaluated using the kNN classifier only, as it achieved the highest baseline concordance and was therefore the most informative platform for assessing whether spatial refinement could improve classification. Cases were selected for enrichment if their whole-slide kNN confidence score fell below a threshold of 0.8, indicating suboptimal classifier confidence. The threshold approximates the mean concordant kNN score (0.846).

Twenty-seven cases fell below the threshold; two control cases were excluded as they contain no neoplastic component. For each qualifying case ($n = 25$; comprising 22 high-grade gliomas, 2 low-grade gliomas/glioneuronal tumors, and 1 medulloblastoma), graph-based clustering was performed on the filtered feature–barcode expression matrix using the Leiden algorithm in Scanpy at a resolution of 0.8 [13] Spatial cluster maps were reviewed by S.J.A. to identify clusters corresponding to tumor-enriched regions based on spatial concordance with expected histological features.

Barcodes from the selected clusters were passed through the same pseudobulk pipeline and QC thresholds used for the whole-slide analysis. The resulting enriched pseudobulk profile was re-

classified through the correlation-based kNN pipeline, and the resulting confidence scores and concordance status were compared with the original whole-slide classifications.

Statistical Analysis

Concordance was the proportion of cases correctly classified, reported for the full cohort and stratified by diagnostic category and preservation type with Wilson 95% confidence intervals. Because diagnostic categories were markedly imbalanced (47 high-grade gliomas versus 4 medulloblastomas), balanced accuracy — the unweighted mean of per-class concordance rates — is reported alongside overall concordance. Classifier confidence scores were reported as the mean with standard deviation (SD) in parentheses, separately for concordant and discordant cases. Confusion matrices for each classifier are provided in Online Resource 3. No formal hypothesis testing was performed as the study is descriptive.

Results

Overall Classifier Performance

Across the 79 cases, the three classifiers demonstrated different concordance rates, with kNN attaining the highest scores, followed by M&M and then OTTER (Fig. 1). The kNN classifier achieved the highest concordance, correctly classifying 65 of 79 cases (82.3%; 95% CI 72.4–89.1), followed by M&M with 44 of 73 analyzable cases (60.3%; 95% CI 48.8–70.7) and OTTER with 33 of 71 (46.5%; 95% CI 35.4–58.0). Because the diagnostic categories were imbalanced, balanced accuracy was also calculated: 92.0% for kNN, 84.6% for M&M and 49.8% for OTTER. Confidence scores tracked concordance, most clearly for kNN, where concordant cases scored

0.846 (0.186) and discordant cases 0.607 (0.230); then M&M, 0.636 (0.282) versus 0.317 (0.160); and least OTTER, 0.409 (0.231) versus 0.333 (0.186) (Online Resource 5).

Diagnosis-Dependent Classification Performance

Classifier performance varied substantially by diagnostic category, with medulloblastoma and ependymoma achieving consistently high concordance across all three tools, while high-grade gliomas and control tissue represented the most challenging groups (Fig. 2a).

Medulloblastoma and ependymoma. All four medulloblastoma cases were classified concordantly by kNN, M&M, and OTTER (4/4, 100%). Where reference annotation specified a molecular subgroup, classifiers with subgroup resolution assigned it correctly (SHH-activated). Similarly, kNN and M&M achieved 100% concordance across all 14 ependymoma cases (mean scores 0.993 and 0.965 respectively), and were also concordant at subgroup level where annotation permitted. OTTER was concordant in 12 of 14 (85.7%).

Low-grade glioma/glioneuronal tumors. kNN classified 7 of 8 correctly (87.5%) and M&M 8 of 8 (100%); OTTER was concordant in only 2 of 8 (25.0%).

High-grade glioma. This was the largest and most challenging diagnostic group (n = 47). The kNN classifier classified 34 of 47 cases correctly (72.3%). M&M reached 38.3% (18/47) and OTTER 38.5% (15/39 analyzable). Notably for OTTER, discordant high-grade glioma cases had higher mean scores (0.383) than concordant ones (0.255), indicating that OTTER confidence scores lack discriminatory validity in this diagnostic group.

Control tissue. kNN classified all 6 cases correctly (100%); M&M has no such category; OTTER classified none concordantly (0/6), a clear limitation for non-neoplastic samples.

Impact of Formalin Fixation on Classification Performance

Concordance and confidence scores were then compared between FF and FFPE material (Fig.2b). The kNN classifier showed a moderate reduction in concordance in FFPE samples (76.7%, 23/30; mean concordant score 0.774 (0.200)) compared to FF samples (85.4%, 41/48; mean concordant score 0.885 (0.170)). M&M concordance was comparable between FF (57.1%, 24/42 analyzable) and FFPE (63.3%, 19/30), though mean concordant scores were markedly lower in FFPE (0.411 vs 0.826), indicating reduced confidence despite similar concordance.

OTTER showed the most striking tissue-preservation effect: concordance fell from 61.4% in FF (27/44 analyzable) to 19.2% in FFPE (5/26 analyzable). Critically, mean scores of discordant FFPE cases, at 0.292 (0.133), were very close to those of concordant cases, at 0.304 (0.229), indicating that OTTER confidence scores carry no meaningful discriminatory information in FFPE material.

Tumor-Cluster Enrichment Improves kNN Classification

Tumor-cluster enrichment was applied to the 25 sub-threshold cases (22 high-grade gliomas, 2 low-grade glioma/glioneuronal tumors, 1 medulloblastoma; Fig. 3, Online Resource 6). Prior to enrichment, 15 of 25 cases were concordantly classified (60.0%), with a mean classifier confidence score of 0.536. Following enrichment, concordance increased to 19 of 25 cases (76.0%), with a mean score of 0.604. Four discordant cases converted to concordant and none became discordant; three of the four were reclassified from low-grade to high-grade glioma. Six remained discordant.

Among the 21 cases with unchanged status, scores improved in 12, with 5 crossing the 0.8 threshold. Per-case results are given in Online Resource 7.

Enrichment was most effective in high-grade glioma, where concordance rose from 13 of 22 (59.1%) to 16 of 22 (72.7%); the already-concordant medulloblastoma's score rose from 0.5 to 1.0. Persistent misclassification was associated with admixed normal or lower-grade tissue, or with intrinsic transcriptomic overlap — exemplified by the gliosarcoma GS7, which retained an ependymoma call despite enrichment.

Application to Institutional Visium HD Cases

The five institutional Visium HD cases were processed through the complete analytical workflow (Fig. 4) and classification results are summarized in Online Resource 8. Both medulloblastoma cases (Group 3 and Group 4) achieved concordant classification across all three classifiers, including correct molecular subgroup assignment (kNN scores 1.0 and 0.9; M&M 0.46 and 0.96; OTTER 0.2 and 0.5 respectively). Notably, the Group 3 medulloblastoma was derived from a tissue fragment less than 1 mm in size. The diffuse pediatric-type high-grade glioma was concordantly classified by M&M (0.12) and OTTER (0.17), though with low confidence scores; the kNN classifier assigned it as a low-grade glioma (0.6). The astroblastoma returned equal kNN scores (0.5) between ependymoma and HGNET-MN1. The embryonal tumor was discordant across all three classifiers, as expected given its absence from all reference datasets.

Discussion

In settings where the specimen volume is limited and when there is dilution of tumor signal, our results show that pseudobulk aggregation of spatial transcriptomics can yield diagnostically informative classifications through existing classifiers from a single tissue section. However, concordant scores show variation depending on classifier architecture, tumor type and preservation.

Classifier performance and the feasibility of pseudobulk classification

Applying three classifiers revealed informative differences in their tolerance of spatial input. kNN achieved the highest concordance (82.3%), attributable to correlation-based matching against the Le et al. atlas: Pearson correlation captures relative expression patterns rather than absolute magnitudes, and is therefore tolerant of platform differences. This scale invariance suits cross-platform application, where systematic biases shift expression levels but preserve relative gene rankings; the atlas's dense sampling of nervous system tumors further supports accurate matching.

M&M's intermediate concordance (60.3%) likely reflects training on a reference enriched for pediatric entities, limiting sensitivity for adult-type tumors — particularly glioblastoma, the largest subgroup here. OTTER's lower concordance (46.5%) is consistent with its design as a deep-learning classifier trained on poly(A)-selected, fresh-frozen RNA-seq data processed through specific bioinformatic pipelines (RSEM quantification with Bowtie2/STAR alignment).[9] Convolutional networks do encode technical signatures of their training modality, and therefore, the different library chemistry, UMI-based quantification and capture efficiency of spatial transcriptomics deviate substantially from those conditions.

The divergence between overall concordance and balanced accuracy is itself informative: kNN (82.3% vs 92.0%) and M&M (60.3% vs 84.6%) both performed well across most categories but poorly on high-grade glioma, the majority of the cohort, whereas OTTER's two measures were close (46.5% and 49.8%), indicating failure spread across several categories.

Diagnosis-dependent performance and clinical implications

The high concordance for medulloblastoma (100%) and ependymoma (≥85.7%) reflects their distinctive transcriptomic signatures, which separate well even across platforms, suggesting pseudobulking spatial classification is readily deployable for posterior fossa tumors.[1]

In contrast, high-grade gliomas were the hardest category for kNN and M&M and were poorly classified by OTTER as well (kNN 72.3%, M&M 38.3%, OTTER 38.5%). This reflects their transcriptomic heterogeneity and overlap with other categories in the reference datasets. High-grade gliomas are also the tumors most likely to infiltrate diffusely, diluting the neoplastic signal in a whole-slide pseudobulk — the problem the enrichment strategy addresses (see below).

Impact of tissue preservation and implications for archival material

FFPE is the standard archival format in surgical neuropathology, so any transcriptomic diagnostic must contend with FFPE-associated RNA degradation, cross-linking and fragmentation. [6,3] The kNN classifier was moderately affected by FFPE processing (concordance 76.7% versus 85.4% in FF), likely because correlation-based confidence is partially robust to the systematic transcript degradation. M&M showed near-identical concordance (57.1% vs 63.3%), indicating reasonable concordance similarity despite reduced signal quality. OTTER showed a dramatic decline from 61.4% concordance in FF to 19.2% in FFPE, with near-complete loss of discriminatory power in

its confidence scores. This appears consistent with OTTER's dependence on the technical characteristics of poly(A)-selected, fresh-frozen RNA-seq data.[5] That kNN and M&M remain concordant on FFPE material supports the feasibility of transcriptomic classification from routine histopathological sections.

Tumor-cluster enrichment as a spatial refinement strategy

Unlike macrodissection or laser-capture microdissection, which consume additional tissue, spatial transcriptomics isolates tumor-enriched regions computationally from a single section. In our analysis, enrichment converted 4 of 10 previously discordant cases to concordant classification, raising overall concordance from 60.0% to 76.0% in the sub-threshold cohort. The most common pattern of correction—reclassification from erroneous low-grade glioma labels to the correct high-grade glioma diagnosis—shows that non-neoplastic (or lower-grade) transcriptomic signals can dominate the whole-slide pseudobulk in these cases and spatial isolation of tumor clusters effectively removes this confounding signal.

However, enrichment did not uniformly improve performance: three concordant high-grade gliomas each lost 0.1 of their score (Fig 3b). Such occurrences likely stem from bulk RNA-seq trained classifiers where tissue containing non-neoplastic components such as necrosis, contributes to the histological classification of high-grade glioma. This is seen in GS6, where the necrotic cluster was required for a higher score (Online Resource 10). Excluding such components, therefore, removes features the classifier associates with the correct diagnosis — a principled limit of in silico enrichment applied to bulk-trained models.

It is also noted that six cases remained discordant despite enrichment, likely indicative of misclassifications arising from intrinsic transcriptomic overlap between the tumor and incorrect reference categories rather than from signal dilution.

Institutional Visium HD validation

The five institutional Visium HD cases demonstrate that the pseudobulk pipeline can extend to a multiplexed workflow in which multiple small specimens are processed simultaneously on a single capture area, reducing per-case cost and maximizing diagnostic yield from limited tissue. The concordant classification of both medulloblastomas — including one derived from a tissue fragment less than 1 mm — suggests the spatial pseudobulk approach does not require large tissue volumes to generate sufficient transcriptomic signal, consistent with the robust medulloblastoma concordance observed in the public cohort. The low confidence for the diffuse pediatric-type high-grade glioma likely reflects both its heterogeneity and the residual platform gap. The embryonal tumor was discordant across all three classifiers — expected for an entity absent from every reference set, and a direct demonstration of how far reference coverage constrains these tools.

Transcriptomic biology validated through spatial classification

During the analysis, it was notable that the classification of several individual cases appears to reflect underlying tumor biology. Four gliosarcoma cases were classified as osteosarcoma or sarcoma groups by M&M and OTTER (Online Resource 9), which supports the understanding of sarcomatous transformation in these tumors.[16] Similarly informative was the astroblastoma with *MN1::BEND2* fusion which returned equal kNN scores for ependymoma and HGNET-MN1 (high-grade neuroepithelial tumor with *MN1*-alteration, its former classification group). This result is

notable considering recent evidence that some *MN1::BEND2*-fused tumors are ependymal in origin.[8] Overall, this suggests that the pseudobulk approach has the potential to capture biologically meaningful transcriptomic relationships even when formal concordance criteria are not met.

Relationship to existing diagnostic adjuncts

When considering current clinical testing modalities, immunohistochemistry and DNA methylation profiling typically require multiple sections with adequate tumor content, a limitation when biopsy material is scarce.[4] NePSTA, a previously published spatial transcriptomic framework, addresses this by training graph neural networks directly on spatial data to predict methylation-based subclasses on a single tissue section.[11]

Our approach is complementary: rather than building a new spatial classifier, it reshapes spatial counts into a bulk-like profile usable by existing frameworks and their reference atlases. NePSTA and our approach are therefore not mutually exclusive — pseudobulk classification offers a rapid first pass, and spatially aware models such as NePSTA could refine it from the same dataset.

Limitations

First, concordance was assessed across five broad categories rather than at subtype level, a consequence of harmonizing classifiers that use different nomenclatures. Regardless, where subgroup annotation existed, predictions remained concordant at that level, suggesting that finer resolution is achievable. Second, the design is descriptive, and subgroup sizes preclude formal comparison, where differences are indicative but not established benchmarks. Third, the cohort is mostly previously published data which permits reproducibility and avoids single-institution bias,

but limits control over specimen handling, sequencing depth and annotation quality. Reference-label errors also propagate directly into concordance.

Fourth, no bulk RNA-seq was run on the same specimens, so output was compared against the histopathological diagnosis. This shows whether pseudobulk profiles yield the correct diagnosis but cannot separate a poorly representative profile from a classifier limitation. Fifth, the study was restricted to Visium and Visium HD platforms and may not generalize to other spatial technologies such as GeoMx or Stereo-seq.[10] Finally, the tumor-cluster enrichment strategy relied on manual review of spatial cluster maps, introducing a subjective element to the analysis.

Conclusion

With our findings, we conclude that in clinical settings where there is a constraint in tissue availability, pseudobulk aggregation of spatial transcriptomics offers a route to transcriptomic-level classification from a single tissue section.

Data and Code availability

The 101 publicly available Visium datasets were obtained from Zenodo (DOI: 10.5281/zenodo.10863259 and 10.5281/zenodo.14064047), Dryad (DOI: 10.5061/dryad.h70rxwdmj) and GEO (GSE195661). The five institutional Visium HD datasets are available from the corresponding author upon reasonable request. The transcriptomic atlas reference data and metadata used for the correlation-based kNN classifier are available at https://github.com/axitamm/BrainTumorAtlas. The M&M classifier and pre-trained models are available at https://github.com/princessmaximacenter/MnM and on Zenodo (DOI: 10.5281/zenodo.14167359). The OTTER classifier is accessible at

https://otter.ccm.sickkids.ca/app/inference. The code used for generating the pseudobulk profiles and results is available from the corresponding author upon reasonable request.

Acknowledgements

We thank Ufuk Degirmenci and his team at Next Level Genomics Pte. Ltd. for performing the Visium HD run. Sequencing of the five institutional cases was supported by the KK Women's and Children's Hospital Health Services Innovation and Development Fund [KKHHF/IDF/2024/08].

Conflict of interest

The authors declare that they have no competing interests.

Declaration of generative AI and AI-assisted technologies in the manuscript preparation process

AI tools were used to assist with drafting analysis code and with manuscript editing. The authors reviewed all output and take full responsibility for the content of this article.

References

1. Arora S, Nuechterlein N, Jensen M et al. (2026) Integrated transcriptomic landscape of medulloblastoma and ependymoma reveals novel tumor subtype-specific biology. Neuro Oncol 28 (2):505-519. doi:10.1093/neuonc/noaf251

2. Aw SJ, Tan EEK, Low SYY et al. (2024) CNS embryonal tumour with concomitant novel BRD4::CTRC1 fusion and BCOR internal tandem duplication - evidence for synergism and non-

377 mutually exclusive alterations in CNS embryonal tumours. Acta Neuropathol Commun 12 (1):33.
378 doi:10.1186/s40478-024-01741-y
379 3. Bossel Ben-Moshe N, Gilad S, Perry G et al. (2018) mRNA-seq whole transcriptome profiling
380 of fresh frozen versus archived fixed tissues. BMC Genomics 19 (1):419. doi:10.1186/s12864-
381 018-4761-3
382 4. Capper D, Jones DTW, Sill M et al. (2018) DNA methylation-based classification of central
383 nervous system tumours. Nature 555 (7697):469-474. doi:10.1038/nature26000
384 5. Comitani F, Nash JO, Cohen-Gogo S et al. (2023) Diagnostic classification of childhood cancer
385 using multiscale transcriptomics. Nat Med 29 (3):656-666. doi:10.1038/s41591-023-02221-x
386 6. Esteve-Codina A, Arpi O, Martinez-Garcia M et al. (2017) A Comparison of RNA-Seq Results
387 from Paired Formalin-Fixed Paraffin-Embedded and Fresh-Frozen Glioblastoma Tissue Samples.
388 PLoS One 12 (1):e0170632. doi:10.1371/journal.pone.0170632
389 7. Le CH, Nelson AK, Berrones AJ et al. (2025) A clinically annotated transcriptomic atlas of
390 nervous system tumors. Neuro Oncol 27 (10):2605-2616. doi:10.1093/neuonc/noaf130
391 8. Lehman NL (2023) Early ependymal tumor with MN1-BEND2 fusion: a mostly cerebral tumor
392 of female children with a good prognosis that is distinct from classical astroblastoma. J Neurooncol
393 161 (3):425-439. doi:10.1007/s11060-022-04222-1
394 9. Li B, Dewey CN (2011) RSEM: accurate transcript quantification from RNA-Seq data with or
395 without a reference genome. BMC Bioinformatics 12:323. doi:10.1186/1471-2105-12-323
396 10. Lim HJ, Wang Y, Buzdin A, Li X (2025) A practical guide for choosing an optimal spatial
397 transcriptomics technology from seven major commercially available options. BMC Genomics 26
398 (1):47. doi:10.1186/s12864-025-11235-3

11. Ritter M, Blume C, Tang Y et al. (2025) Spatially resolved transcriptomics and graph-based deep learning improve accuracy of routine CNS tumor diagnostics. Nat Cancer 6 (2):292-306. doi:10.1038/s43018-024-00904-z

12. Stahl PL, Salmen F, Vickovic S et al. (2016) Visualization and analysis of gene expression in tissue sections by spatial transcriptomics. Science 353 (6294):78-82. doi:10.1126/science.aaf2403

13. Traag VA, Waltman L, van Eck NJ (2019) From Louvain to Leiden: guaranteeing well-connected communities. Sci Rep 9 (1):5233. doi:10.1038/s41598-019-41695-z

14. Wallis FSA, Baker-Hernandez JL, van Tuil M et al. (2025) M&M: an RNA-seq based pan-cancer classifier for paediatric tumours. EBioMedicine 111:105506. doi:10.1016/j.ebiom.2024.105506

15. WHO Classification of Tumours Editorial Board (2021) Central nervous system tumours

16. Wojtas B, Gielniewski B, Wojnicki K et al. (2019) Gliosarcoma Is Driven by Alterations in PI3K/Akt, RAS/MAPK Pathways and Characterized by Collagen Gene Expression Signature. Cancers (Basel) 11 (3). doi:10.3390/cancers11030284

17. Wolf FA, Angerer P, Theis FJ (2018) SCANPY: large-scale single-cell gene expression data analysis. Genome Biol 19 (1):15. doi:10.1186/s13059-017-1382-0

Figure legends

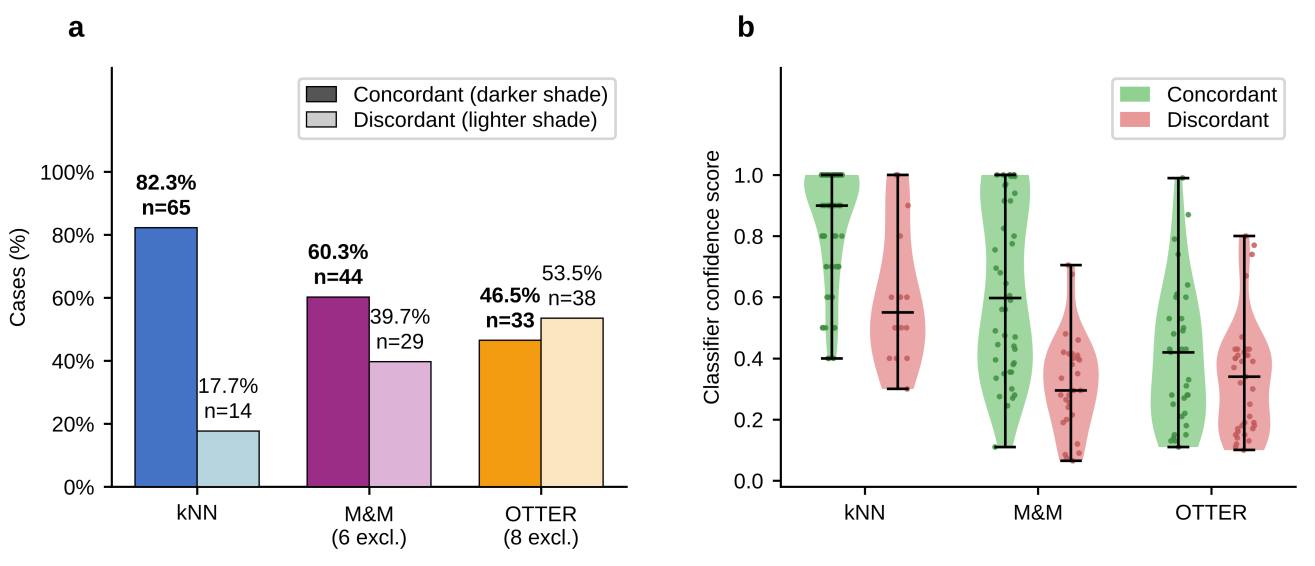
Fig. 1 Overall performance of three spatial transcriptomic classifiers across the cohort. a Concordance rate for kNN, M&M and OTTER across the 79 spatially profiled tumor and control samples; concordant (darker) and discordant (lighter) proportions are annotated above each bar

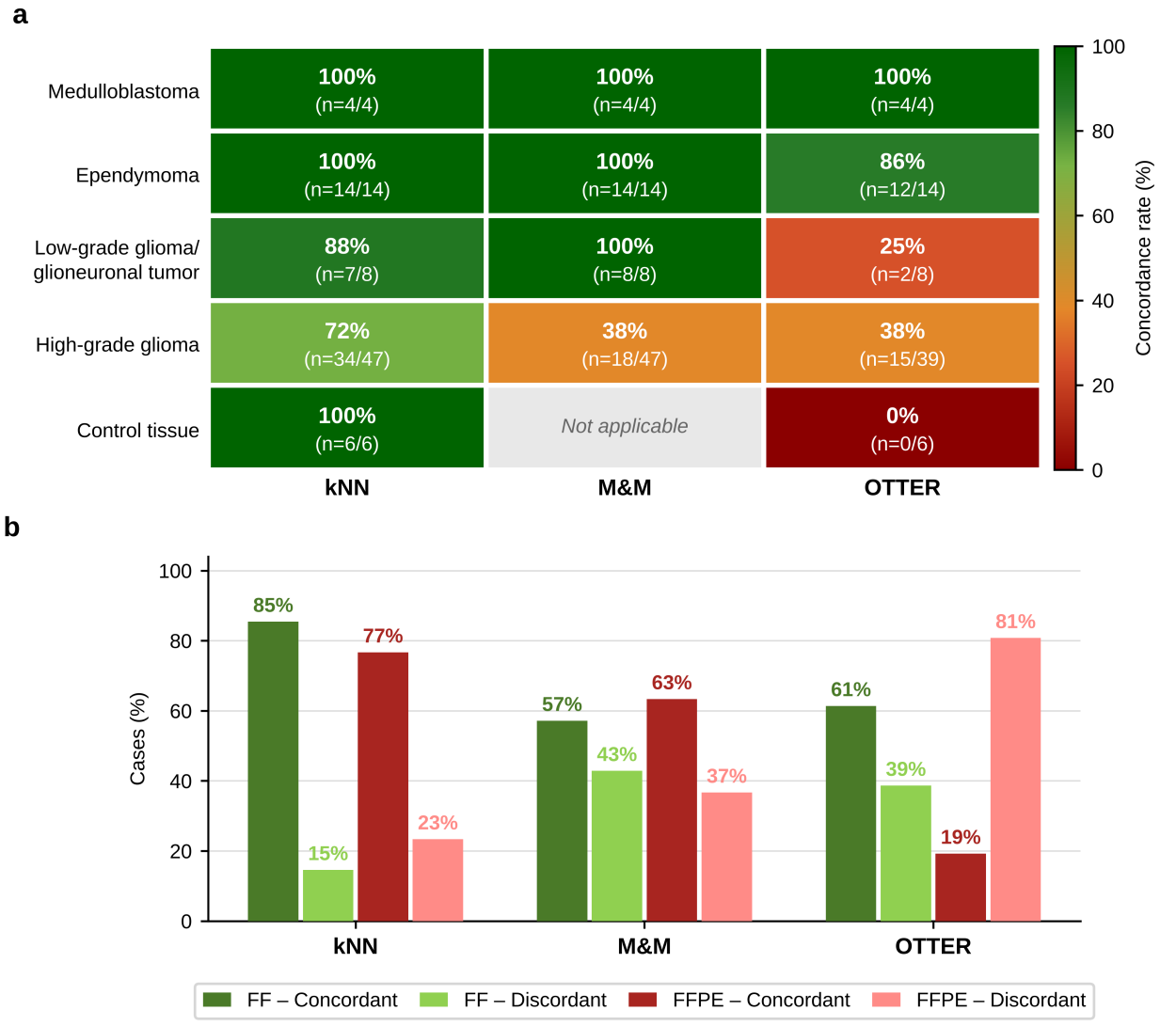
pair. Denominators differ because 6 control cases lie outside the M&M reference and 8 gliomas returned an unresolved OTTER node (n = 73 and n = 71 respectively). **b** Confidence scores for concordant (green) and discordant (red) cases as paired violin plots with individual points overlaid. Separation of concordant from discordant scores is marked for kNN, partial for M&M and poor for OTTER.

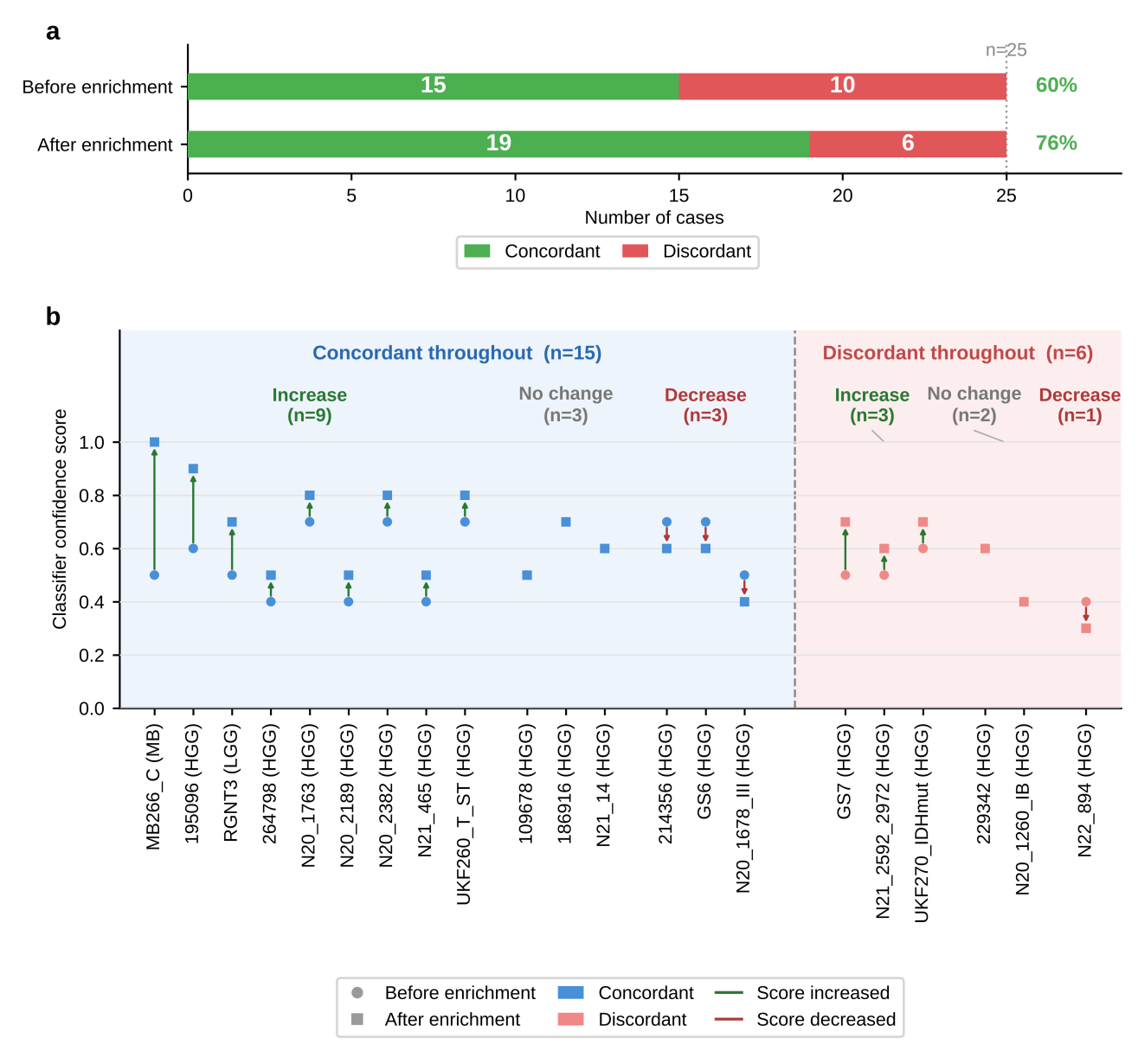
Fig. 2 Diagnosis-dependent and tissue preservation-dependent classifier performance. a Concordance rate (%) by diagnostic category; cell color runs from red (0%) to dark green (100%). b Concordance rate in fresh-frozen (FF) and formalin-fixed paraffin-embedded (FFPE) material. Analyzable denominators: kNN FF n = 48, FFPE n = 30; M&M FF n = 42, FFPE n = 30; OTTER FF n = 44, FFPE n = 26.

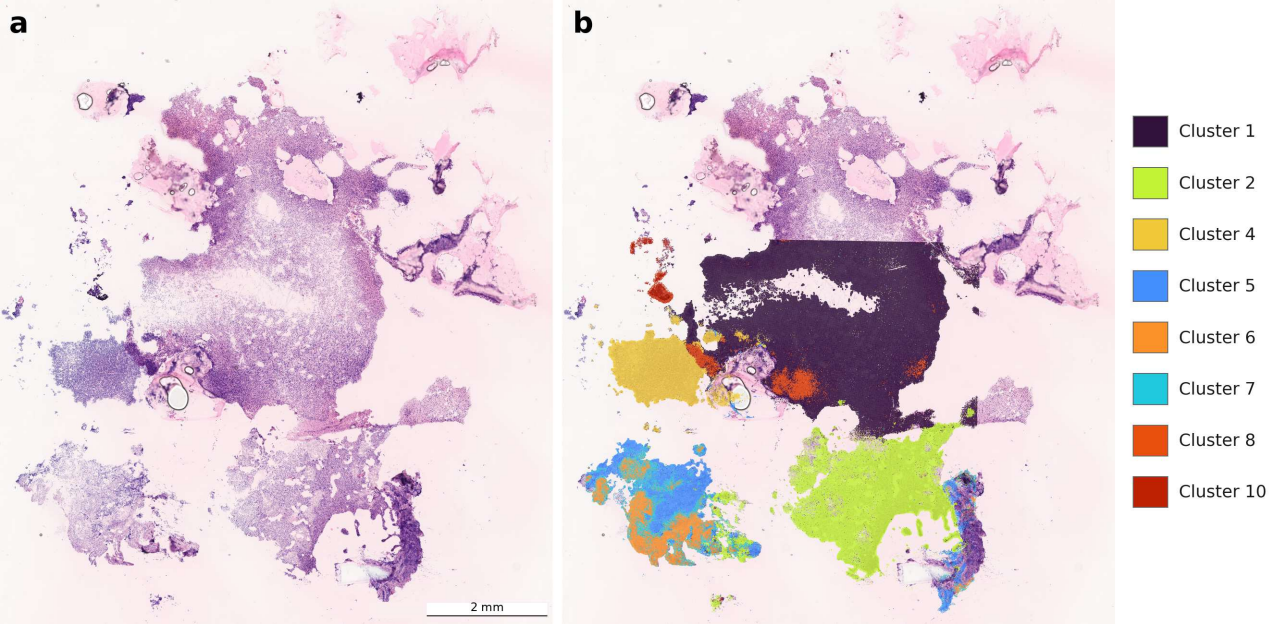
Fig. 3 Effect of tumor-cluster enrichment on kNN classification in the 25 sub-threshold cases. **a** Concordance before and after enrichment. **b** kNN score before (circles) and after (squares) enrichment for the 21 cases whose concordance status was unchanged; subgroup labels give the number of cases in which the score rose, was unchanged or fell.

Fig. 4 Institutional Visium HD cases. H&E (**a**) and spatial clusters (**b**) for the five cases, rendered in Loupe v9.0.0. Clusters 1 and 8, diffuse pediatric-type high-grade glioma, H3-wildtype and IDH-wildtype; cluster 2, astroblastoma; cluster 4, medulloblastoma group 4; clusters 5, 6 and 7, embryonal tumor with *BRD4::CTRC1* fusion and *BCOR* internal tandem duplication; cluster 10, medulloblastoma group 3. Classifications are given in Online Resource 8.


a
Concordant (darker shade)
Discordant (lighter shade)
Cases (%)
100%
80%
60%
40%
20%
0%
82.3%
n=65
17.7%
n=14
60.3%
n=44
39.7%
n=29
46.5%
n=33
53.5%
n=38
kNN
M&M
(6 excl.)
OTTER
(8 excl.)
b
Concordant
Discordant
Classifier confidence score
1.0
0.8
0.6
0.4
0.2
0.0
kNN
M&M
OTTER


a
Medulloblastoma
Ependymoma
Low-grade glioma/ glioneuronal tumor
High-grade glioma
Control tissue
100% (n=4/4)
100% (n=4/4)
100% (n=4/4)
100% (n=14/14)
100% (n=14/14)
86% (n=12/14)
88% (n=7/8)
100% (n=8/8)
25% (n=2/8)
72% (n=34/47)
38% (n=18/47)
38% (n=15/39)
100% (n=6/6)
Not applicable
0% (n=0/6)
kNN
M&M
OTTER
Concordance rate (%)
100
80
60
40
20
0
b
Cases (%)
100
80
60
40
20
0
85%
15%
77%
23%
57%
43%
63%
37%
61%
39%
19%
81%
kNN
M&M
OTTER
FF – Concordant
FF – Discordant
FFPE – Concordant
FFPE – Discordant


a
n=25
Before enrichment
After enrichment
15
10
19
6
60%
76%
0
5
10
15
20
25
Number of cases
Concordant
Discordant
b
Concordant throughout (n=15)
Discordant throughout (n=6)
Increase (n=9)
No change (n=3)
Decrease (n=3)
Increase (n=3)
No change (n=2)
Decrease (n=1)
Classifier confidence score
1.0
0.8
0.6
0.4
0.2
0.0
MB266_C (MB)
195096 (HGG)
RGNT3 (LGG)
264798 (HGG)
N20_1763 (HGG)
N20_2189 (HGG)
N20_2382 (HGG)
N21_465 (HGG)
UKF260_T_ST (HGG)
109678 (HGG)
186916 (HGG)
N21_14 (HGG)
214356 (HGG)
GS6 (HGG)
N20_1678_III (HGG)
GS7 (HGG)
N21_2592_2972 (HGG)
UKF270_IDHmut (HGG)
229342 (HGG)
N20_1260_IB (HGG)
N22_894 (HGG)
Before enrichment
After enrichment
Concordant
Discordant
Score increased
Score decreased


a
b
2 mm
Cluster 1
Cluster 2
Cluster 4
Cluster 5
Cluster 6
Cluster 7
Cluster 8
Cluster 10

Supplementary Files

This is a list of supplementary files associated with this preprint. Click to download.

- ESM2.xlsx
- ESM1.docx
- ESM3.pdf
- ESM4.pdf
- ESM5.xlsx
- ESM6.pdf
- ESM8.xlsx
- ESM9.xlsx
- ESM7.docx
- ESM10.pdf